Theoretical and Experimental Study of the Diffraction Contrast on Magnetic Domain Walls

M. Polcarová and J. Brádler
Institute of Physics, Czechoslovak Academy of Sciences, Prague

Z. Naturforsch. **37a**, 419–426 (1982); received December 23, 1981

Dedicated to Prof. Dr. G. Hildebrandt on the occasion of his 60th birthday

Dynamical theory of the X-ray diffraction on a crystal containing misfit boundary was applied to the interpretation of the contrast observed in X-ray topographs on 90° magnetic domain walls in single crystals of an Fe-Si alloy. The integrated intensities were computed for several cases corresponding to the actual conditions of experiments. Good agreement of theoretical and experimental results was obtained.

Introduction

X-ray diffraction contrast on magnetic domain structures arises as a consequence of magnetostriction. Greatest attention was paid to the interpretation of the contrast on domains in Fe-Si single crystals (e.g. [1–6]). A strong contrast appears on 90° domain walls due to an abrupt change of the magnetostrictive deformation. The diffracting conditions of the wave field propagating through the crystal vary across the domain wall and the intensities of the exit beams differ from those of the perfect crystal.

It was shown [1] that the contrast appears if

$$(\boldsymbol{m}_2 - \boldsymbol{m}_1)\,\boldsymbol{H} \neq 0\,, \tag{1}$$

where $\boldsymbol{m}_1$ and $\boldsymbol{m}_2$ are unit vectors parallel to the direction of magnetization in the adjacent domains and $\boldsymbol{H}$ is the diffraction vector.

This result is consistent with the model of a 90° domain wall parallel to the (110) plane as a coherent twinning boundary [1, 4]. The planes of the zone $\boldsymbol{m}_2 - \boldsymbol{m}_1$ are not affected by the wall, whereas the orientation and/or interplanar spacing of the others change across the wall; this change depends on the value of the magnetostrictive constant λ_{100}. This model was directly verified by measurement on a double crystal spectrometer [7].

Diffraction contrast due to a (110) 90° domain wall was studied in more detail on single crystal plates parallel to the (001) plane using reflection on $(1\bar{1}0)$ planes normal to the wall [4]. The diffracting planes are tilted by an angle of $3\lambda_{100}$ across the wall, their interplanar distance remains constant. For taking the topographs, the sample was rotated by an angle up to 30° around the diffraction vector with respect to the usual vertical position. The walls, normal to the surface, appear then on the topographs as bands having a width equal to $T_0 \sin\alpha$, α being the rotation angle. They are dark, i.e., the diffracted intensity is higher than that from the perfect crystal if the product (1) is positive, and light if this expression is negative. The diffracted intensity was calculated theoretically under simplified conditions and a qualitative agreement was achieved [4, 8].

A further step was made by comparing the contrast in the diffracted and forward diffracted beams [9]. It was shown, that the wall image in the forward diffracted beam is always lighter than the perfect crystal. In contradistinction to the diffracted beam, the band forming the wall image is not symmetrical, but it is darker at the entrance surface and lighter at the exit surface, if (1) is >0 and vice versa. These experimental results agree with the theoretical considerations based on the simplified calculations.

The aim of this paper is to present the results of the exact calculations of the diffracted and forward diffracted intensities on the wall done for parameters corresponding to the actual experimental conditions and their comparison with experiments.

Reprint requests to Dr. M. Polcarová, Institute of Physics, Czech. Acad. Sci., Na Slovance 2, 180 40 Prague 8, Czechoslovakia.

0340-4811 / 82 / 0500-0419 $ 01.30/0. — Please order a reprint rather than making your own copy.

Theory

A general dynamical theory of X-ray diffraction on a crystal containing a misfit boundary was developed in [10]. The crystal was supposed to be perfect except for a single fault plane where the direction and/or the absolute value of the diffraction vector $\boldsymbol{H}$ change. Laue case of diffraction with respect to both the surface and the interface was considered. New waves appear in the second part of the crystal giving rise to interferences. Equations of all diffracted and forward diffracted waves including phases and absorption were derived.

A 90° domain wall can be treated as a special case of the misfit boundary — a coherent boundary. Under our experimental conditions, symmetrical Laue case with respect to both the surface and the interface takes place and $|\boldsymbol{H}|$ is constant, i.e., only the direction of the diffraction vector changes. Then the equations simplify to the form presented in [10], Part III with

$$|\delta(\Delta\vartheta)| = |\delta\vartheta| = 3\lambda_{100}|\sin\alpha|,$$

$\delta(\Delta\vartheta)$ being the change of the deviation $\Delta\vartheta$ of the glancing angle ϑ from the Bragg angle ϑ_B, $\Delta\vartheta = \vartheta - \vartheta_B$. The sign of $\delta(\Delta\vartheta)$ corresponds to that of (1).

Applying this theory, the following aspects of the domain walls are neglected: 1. The domain wall is in fact not a single fault plane; its thickness l, however, is less than 0.1 μm, i.e. less than the resolving power of X-ray topography. 2. The domain wall is actually not plane, but zigzaged [11, 12]. Following [12], such a wall can be treated as a row of parallel quasi-twist disclination lines of alternating signs. That means that the long range stresses from the adjacent wall junctions are rapidly screened. Possible effect of zigzags on the contrast will be discussed later.

The strain gradient $\delta(\Delta\vartheta)/l$ is larger than 1 cm^{-1}, i.e. much larger than the ratio of the reflection width over the Pendellösung period $\sim 10^{-2}$ cm^{-1}. That means that, according to [13], the conditions for the creation of new waves at the wall is fulfilled.

The integrated intensities

$$R_0 = \frac{1}{I_i}\int_{-\infty}^{\infty}\left[I_0 - \exp\left(-\frac{\mu_0 T}{\cos\vartheta_B}\right)\right]d\eta$$

and

$$R_H = \frac{1}{I_i}\int_{-\infty}^{\infty} I_H\, d\eta,$$

were calculated using the results of [10] for the forward diffracted and diffracted intensities I_0 and I_H; I_i is the intensity of the incident wave, μ_0 is the linear absorption coefficient, $T = T_0/\cos\alpha$ is the effective thickness of the sample, $\eta = \Delta\vartheta/d\mathscr{D}$, d is the interplanar spacing, $1/\mathscr{D}$ is the Pendellösung period.

The intensities were computed as functions of $z = t_f/T$, (t_f is the perpendicular distance of the exit surface from the interface) for the values of μ_0, T, ϑ_B, $\delta\eta = \delta\vartheta/d\mathscr{D}$ corresponding to the actual experimental conditions (see Table 1). Both directions of polarization were taken into account. Numerical integration was carried out for $-50 < \eta < 50$ with precision better than 1%.

The integrated intensities were calculated also approximately using the wave $d_{\alpha\alpha}$ with low anomalous absorption only. This procedure was applied in the previous work [8, 9] and was supposed to be a good approximation for $z = 0.5$ and $\mu_0 T/\cos\vartheta_B > 5$. The same parameters as for exact calculation and the polarization factor $C = 1$ were used. For the forward diffracted intensity the following formula was applied:

$$(R_{\alpha\alpha})_0 = \frac{1}{I_i}\int_{-\infty}^{\infty}(D_{\alpha\alpha})_0^2 \cdot\left\{\exp[-\mu_\alpha T(1-z) - \mu_\alpha' T z] - \exp\left(\frac{\mu_0 T}{\cos\vartheta_B}\right)\right\} d\eta,$$

$D_{\alpha\alpha}$ being the amplitude of the wave with the lowest anomalous absorption, μ_α and μ_α' the absorption coefficients of the first and second crystal region, respectively.

From the calculated intensities the ratio was determined

$$P_i(z, \mu_0 T/\cos\vartheta_B, \mathscr{D}, \delta\eta) = \frac{R_i(z, \mu_0 T/\cos\Theta_B, \mathscr{D}, \delta\eta)}{R_i(z, \mu_0 T/\cos\vartheta_B, \mathscr{D}, 0)},$$

where $R_i(z, \mu_0 T/\cos\vartheta_B, \mathscr{D}, 0)$ is the intensity of the perfect crystal. This quantity can be compared directly with the contrast observed on the topographs.

Experimental

Measurements of the contrast on 90° domain wall were carried out on two specimens prepared from

an Fe-3 wt%Si single crystal grown by the floating-zone technique [14]. The bulk of the crystal was annealed for 50 hs at temperature $\sim 30\,°C$ below the melting point. Plates parallel to the (001) plane were cut, thinned by mechanical polishing and finally chemically polished to remove the surface damage. The final thickness of specimen A was $T_0 = 127\ \mu m$, that of specimen B was $T_0 = 318\ \mu m$. The thicknesses of the samples were determined from the width of the wall image and from the number of the Pendellösung fringes appearing on low angle boundaries [15] with a precision of $\sim 5\ \mu m$.

In order to record the forward diffracted beam without disturbing background from the transmitted short-wavelength radiation a double crystal arrangement had to be used. The integrated intensity was obtained by oscillation of the sample over the rocking curve during the exposure. The topograph taken in the diffracted beam was equivalent to that using the usual Lang method.

A double crystal spectrometer in nearly parallel $(n, -m)$ setting was applied [16, 7]. As the first and second crystals, a perfect Germanium (symmetrical Bragg case, 220 reflection, $d = 0.20003$ nm) and the measured specimen (symmetrical Laue case, $1\bar{1}0$ reflection, $d = 0.20242$ nm) were used. The specimen was inclined around the $\boldsymbol{H}$ vector so that the angle between the surface and vertical direction was 30° (Figure 1). The effective thickness of the specimen is $T_0 \sin \alpha$. Three different wavelengths were used for experiments (AgKα, MoKα, CoKα) to vary the $\mu_0 T$, $\mathscr{D}$ and $\delta\eta$ values (see Table 1). The crystal was oscillated over the range of 37 and 100 secs of arc for MoKα, AgKα and CoKα radiations respectively.

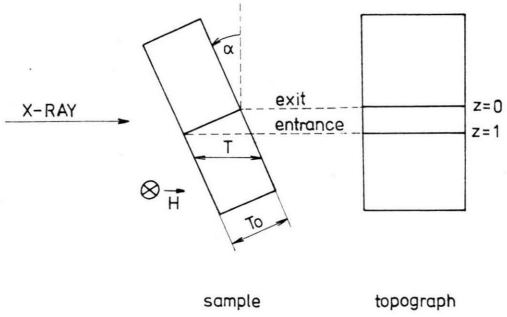

Fig. 1. Projection of the domain wall in the topograph. $z = 0$ and $z = 1$ correspond to the exit and entrance surfaces, respectively.

Table 1. Parameters characterising the diffraction on domain walls.

λ	ϑ_B	$\frac{1}{\mu}$ μm	$\frac{1}{\mathscr{D}}$ μm	$\lvert\delta\eta\rvert$	Λ μm
CoKα	26.22°	22.6	4.72	0.93	3.36
MoKα	10.09°	33.7	10.17	2.01	4.53
AgKα	7.94°	65.8	13.04	2.58	4.71

The topographs of diffracted and forward diffracted beams were recorded on Ilford L4 Nuclear emulsion plates. Special care was taken to use a linear part of the optical density vs. intensity curve of the plates only. For comparison, Lang transmission topographs of both samples were taken as well. The optical density of the images of the domain walls was measured on microdensitometer using 5 μm effective slit width and 10 μm steps. The contrast P was determined as a ratio of the density on the wall image over the density of the perfect crystal.

Results and Discussion

The contrast on domain walls was calculated and measured for two samples and three wavelengths. The six cases thus give a fairly large variety of diffraction conditions (see Table 1, 2). The theoretical results for sample A, CoKα radiation, i.e. medium absorption are shown in Fig. 2, the corresponding topographs are in Figure 3. The contrast values from the measured densities are marked as points in Figure 2. The diffracted intensity for

Table 2. Contrast calculated and measured in the diffracted beam.

λ	$\frac{\mu_0 T}{\cos\vartheta_B}$	$\delta\eta$	P_H calculated		P_H measured	
			P_H	$P_{\alpha\alpha H}$	double	Lang
CoKα	18.12	0.93	0.46	0.46	0.57	0.43
		−0.93	0.08	0.08	0.13	0.17
	7.24	0.93	1.16	1.16	1.24	1.24
		−0.93	0.23	0.23	0.33	0.26
MoKα	11.08	2.01	0.24	0.24	0.45	0.53
		−2.01	0.01	0.01	0.04	0.09
	4.42	2.01	1.11	1.10	1.26	—
		−2.01	0.13	0.07	0.21	—
AgKα	5.58	2.58	0.68	0.69	1.03	1.15
		−2.58	0.06	0.03	0.23	0.15
	2.23	2.58	1.61	1.57	—	1.92
		−2.58	0.48	0.10	—	0.70

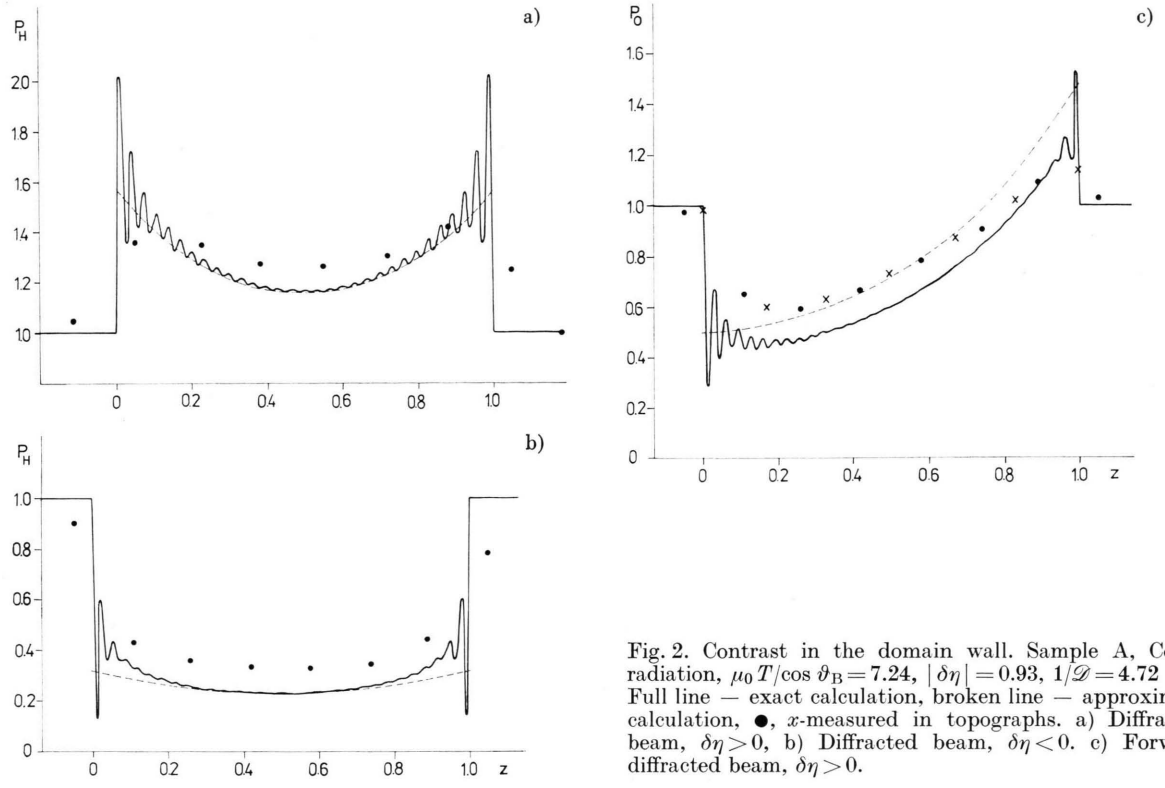

Fig. 2. Contrast in the domain wall. Sample A, CoKα radiation, $\mu_0 T/\cos\vartheta_B = 7.24$, $|\delta\eta| = 0.93$, $1/\mathscr{D} = 4.72$ μm. Full line — exact calculation, broken line — approximate calculation, ●, x-measured in topographs. a) Diffracted beam, $\delta\eta > 0$, b) Diffracted beam, $\delta\eta < 0$. c) Forward diffracted beam, $\delta\eta > 0$.

$\delta\eta > 0$ is higher than that of the perfect crystal with even darker margins at both surfaces (Fig. 2a); that for $\delta\eta < 0$ is lower (Figure 2b). The forward diffracted intensity has the same value in the middle ($z = 0.5$) for both signs of $\delta\eta$, it is however not symmetrical with respect to the surfaces. In Fig. 2c the P vs. z curve for $\delta\eta > 0$ is shown, that for $\delta\eta < 0$ has an opposite shape, i.e. $P(\delta\eta, z) = P(-\delta\eta, 1-z)$. The experimentally determined contrast fits very well with the theoretical curve regarding both its shape over the wall image and the absolute values. The sharp margins are well seen on the topographs, they cannot be, however, measured precisely due to the finite width of the densitometer slit (wall image is only ~ 73 μm wide). The theoretical P vs. z curves show oscillations with

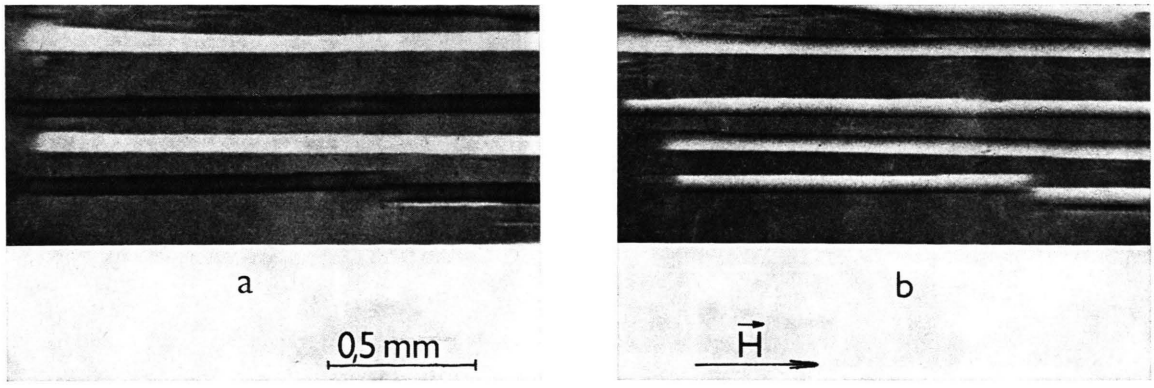

Fig. 3. Double crystal X-ray topographs, sample A, CoKα radiation. The parallel bands are images of 90° walls of alternate signs of $\delta\eta$. The upper and lower edges of the bands correspond to the intersections of the walls with the exit and entrance surfaces, respectively (cf. Figure 1). a) Diffracted beam. b) Forward diffracted beam.

the period $1/\mathscr{D}$ detectable even in the middle of the wall image. That means that with the absorption used, the waves $d_{\alpha\beta}$ and $d_{\beta\alpha}$ still contribute to the intensity and cause interferences. The approximately calculated contrast $P_{\alpha\alpha}$ does not, naturally, show any oscillations nor is it continuous at the surfaces. Its main course agrees with that exactly calculated, the absolute values differ very little for the diffracted beam in the middle of the image and is slightly higher for the forward diffracted beam. The interferences are not visible in the topographs: they are too dense to be resolved (~ 2.4 μm) and superimposed by the image of zigzags [11], slightly visible also in the originals of double crystal topographs.

The second, high absorption case (sample B, MoKα radiation, Fig. 4—6) reveals the same main features with minor differences. The contrast P is less than one even for diffracted beam, $\delta\eta > 0$, except for sharp dark margins. The oscillations appearing at the margins result from interferences of the $d_{\alpha\alpha}$ and $d_{\beta\alpha}$ waves near the entrance surface and $d_{\alpha\alpha}$ and $d_{\alpha\beta}$ waves near the exit surface. Their period equals approximately

$$\Lambda = \frac{1}{\mathscr{D}\sqrt{1+(\delta\eta)^2}},$$

as estimated in [10] (see Table 1 and Figure 6). They fade out very rapidly (for $z < 0.05$ and $z > 0.95$). The $P_{\alpha\alpha}$ approximation coincides with the exactly calculated contrast except for regions near the surfaces.

Other investigated cases give analogical results. They are characterized by numbers summarized in Tables 2, 3. The $P_{\alpha\alpha}$ approximation appears to be satisfactory for the diffracted beam, if

$$\mu_0 T/\cos\vartheta_B > 5$$

and for the forward diffracted beam, if

$$\mu_0 T/\cos\vartheta_B > 10\,.$$

The contrasts calculated for both directions of polarization differ very little in their mean values,

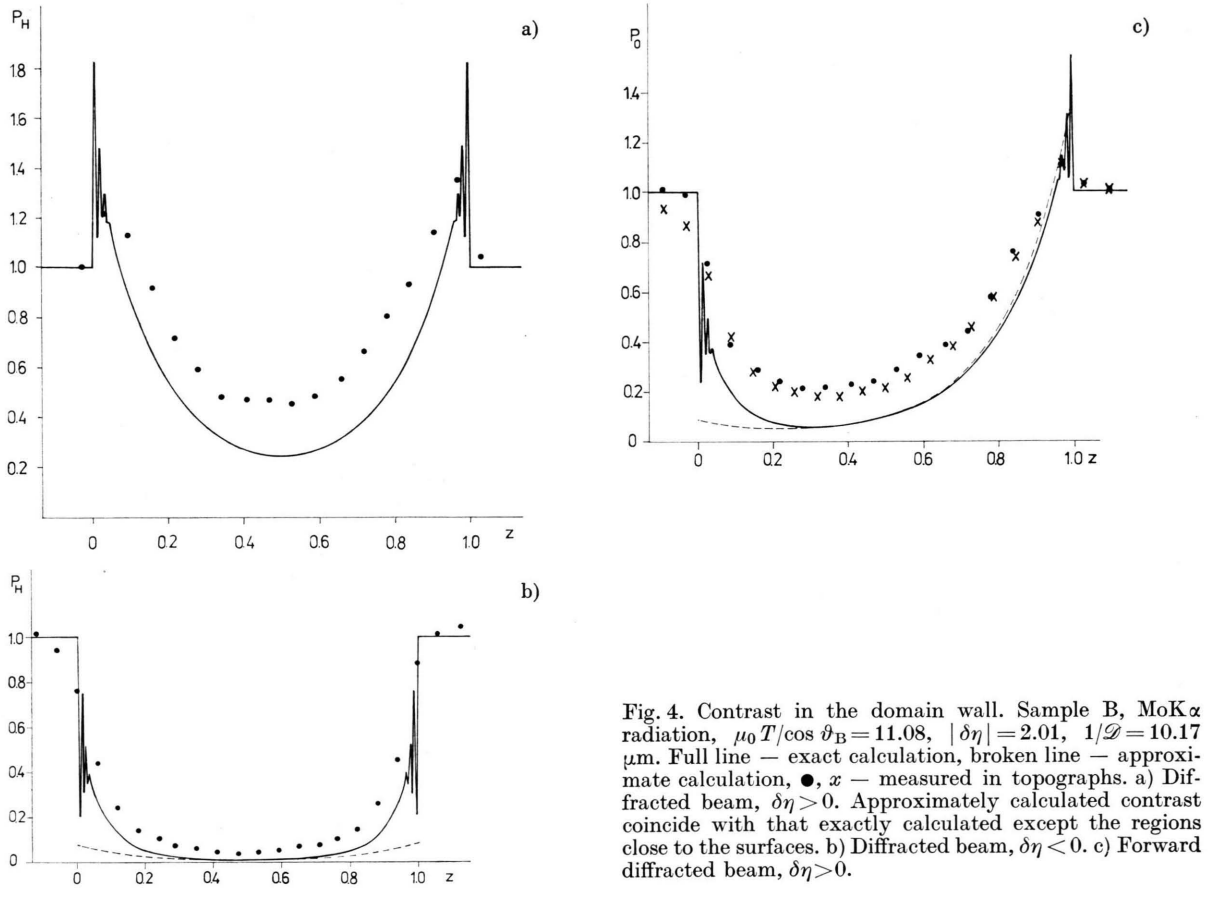

Fig. 4. Contrast in the domain wall. Sample B, MoKα radiation, $\mu_0 T/\cos\vartheta_B = 11.08$, $|\delta\eta| = 2.01$, $1/\mathscr{D} = 10.17$ μm. Full line — exact calculation, broken line — approximate calculation, ●, x — measured in topographs. a) Diffracted beam, $\delta\eta > 0$. Approximately calculated contrast coincide with that exactly calculated except the regions close to the surfaces. b) Diffracted beam, $\delta\eta < 0$. c) Forward diffracted beam, $\delta\eta > 0$.

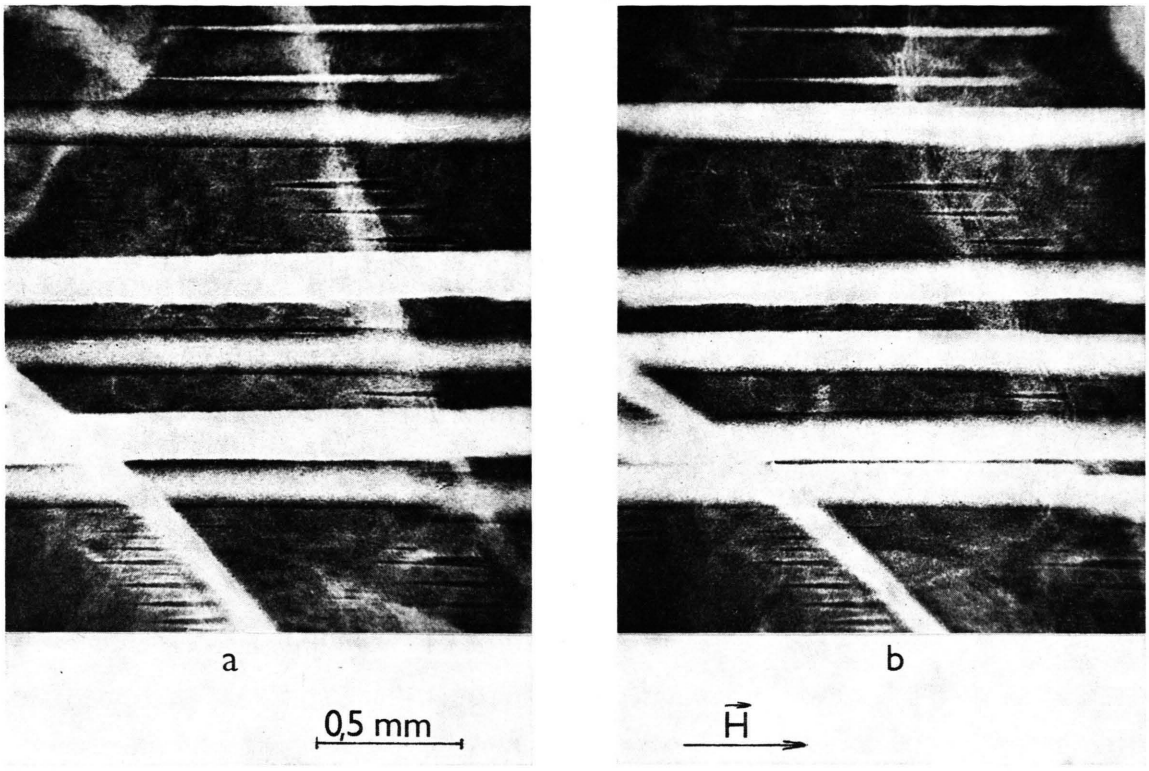

Fig. 5. Double crystal X-ray topographs, sample B, MoKα radiation. The wall images are broader than in Figure 3 because of thicker sample. a) Diffracted beam. b) Forward diffracted beam.

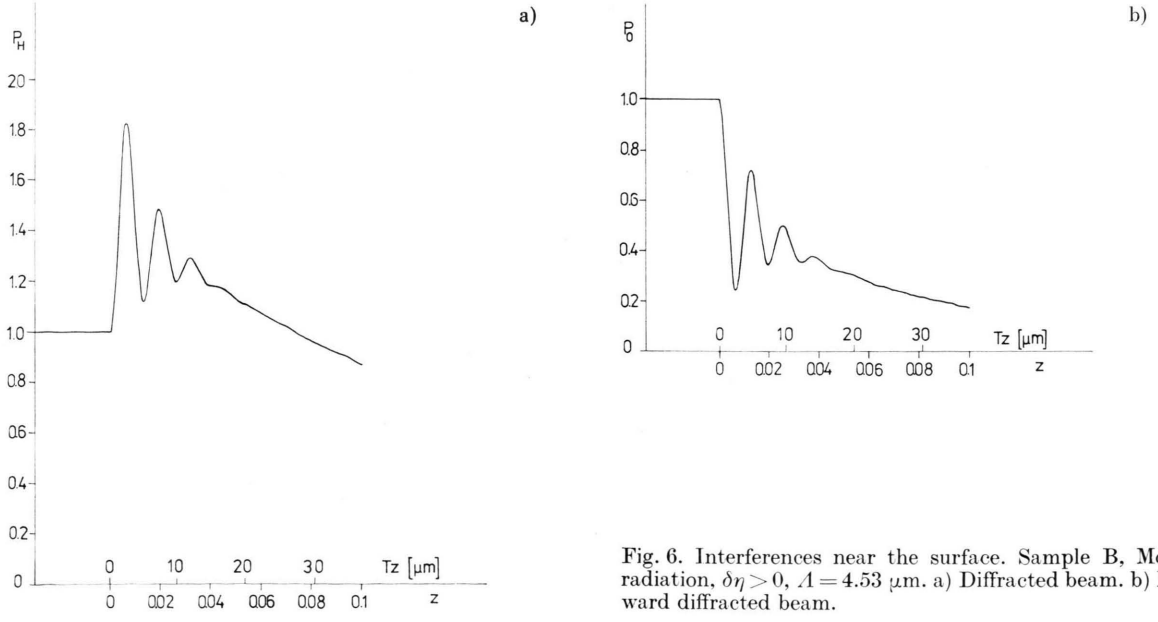

Fig. 6. Interferences near the surface. Sample B, MoKα radiation, $\delta\eta > 0$, $\Lambda = 4.53$ μm. a) Diffracted beam. b) Forward diffracted beam.

λ	$\frac{\mu_0 T}{\cos\vartheta_B}$	calculated, $\delta\eta > 0$				measured
		$P_{0\min}$	$z_{\min}$	P_0 $(z=0.5)$	$P_{\alpha\alpha 0}$ $(z=0.5)$	$P_{0\min}$
CoKα	18.12	0.17	0.31	0.21	0.22	0.25
	7.24	0.45	0.15	0.60	0.71	0.60
MoKα	11.08	0.06	0.29	0.10	0.10	0.19
	4.42	0.34	0.26	0.45	0.74	0.56
AgKα	5.58	0.23	0.30	0.31	0.47	0.53
	2.23	0.09	0.21	0.23	1.05	—

Table 3. Contrast calculated and measured in the forward diffracted beam.

only the interferences in lower absorption cases are affected. Therefore, for the dependence of the contrast on $\delta\eta$ the approximation $P_{\alpha\alpha}$ can be used (Figure 7). This, however, determines only the contrast in the middle of the wall and cannot inform us of the course over the image width, particularly at the margins.

The experimental values of contrast obtained from double crystal and Lang topographs for the diffracted beam and from double crystal topographs for the forward diffracted beam are in the last columns of Tables 2 and 3 respectively. The experimental values are systematically somewhat higher than the theoretical contrast. The reason for this can be as follows:

1. The wall is not plane, but zigzagged. From the considerations based on calculations of strains due to the zigzags [12] no conclusions can be made about the contrast even in a qualitative way. It seems, however, from the observation of Lang topographs that the zigzags may enhance the diffracted intensity.
2. The crystal is not perfect. The irregularly distributed dislocations (mean density $\sim 10^2$ cm^{-2}) lower the intensity due to their dynamical images (see Figures 3, 5). It follows that the intensity determined from the density measured outside the domain walls is lower than that of the perfect crystal and the experimental contrast is higher. The presence of defects is also the most probable reason of the spread of the measured contrast values.
3. The course of the measured contrast over the wall is flattened due to the relatively low resolving power of the densitometer (5—10 μm) with respect to the width of the wall image, especially in the case of sample A.
4. Errors may have arised from not exact knowledge of the sample thicknesses and the tilt angle α.

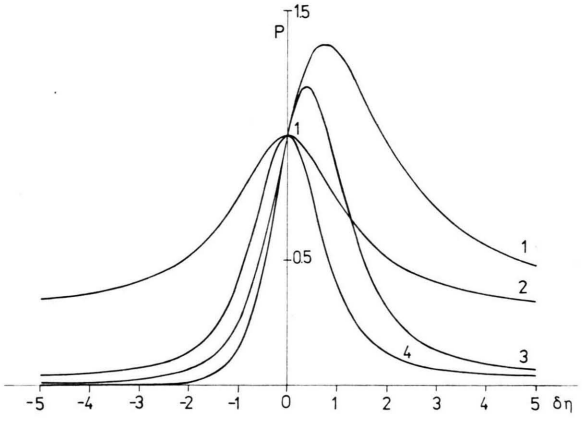

Fig. 7. Dependence of contrast on $\delta\eta$, $z=0.5$. 1, 3 — diffracted beam; 2, 4 — forward diffracted beam. 1, 2 — $\mu_0 T/\cos\vartheta_B = 5$; 3, 4 — $\mu_0 T/\cos\vartheta_B = 10$.

Conclusions

1. Dynamical theory of diffraction on a crystal containing misfit boundary explains satisfactorily the contrast observed on 90° magnetic domain walls in single crystals of Fe-Si alloys. The exact calculations of intensity verify the previous approximate results and give new details.

2. The diffracted intensity for $\delta\eta > 0$ is higher or lower than that of the perfect crystal, depending on the magnitude of $\delta\eta$ and absorption. It is always higher near the intersections of the domain wall with the surfaces. For $\delta\eta < 0$, the diffracted intensity is lower than that of the perfect crystal. The wall image is symmetrical with respect to the surfaces.

3. The forward diffracted intensity is lower than that of the perfect crystal for the middle of the

plate irrespective of the sign of $\delta\eta$ and asymmetrical with respect to the surfaces. It is higher near the entrance surface for $\delta\eta > 0$ and vice versa.

4. Oscillations of the curve of contrast vs. depth below the surface appear as a result of wave interference even in high absorption case, at least near the surfaces.

5. The intensity calculated from the waves with low anomalous absorption only is a good approximation for the middle of the plate and high absorption cases.

6. Experimentally determined contrast fits well with the theoretical curve regarding both the shape and the absolute values. Somewhat higher experimental values can be explained by defects (zigzags, dislocations).

Acknowledgement

The authors are indebted to Dr. V. Kamberský for helpfull discussions and to Dr. J. Gemperlová for valuable comments to the manuscript.

[1] M. Polcarová and J. Kaczér, phys. stat. sol. **21**, 635 (1967).
[2] B. Roessler, phys. stat. sol. **20**, 713 (1967).
[3] M. Schlenker, P. Brissonneau, and J. P. Perrier, Bull. Soc. fr. Minéral. Cristallogr. **91**, 653 (1968).
[4] M. Polcarová and A. R. Lang, Bull. Soc. fr. Minéral. Cristallogr. **91**, 645 (1968).
[5] S. Nagakura and Y. Chikaura, J. Phys. Soc. Japan **30**, 495 (1971).
[6] M. Kléman, M. Labrune, J. Miltat, C. Nourtier, and D. Taupin, J. Appl. Phys. **49**, 1989 (1978).
[7] J. Brádler and M. Polcarová, phys. stat. sol. (a) **9**, 179 (1972).
[8] M. Polcarová, Z. Naturforsch. **28a**, 639 (1973).
[9] M. Polcarová and J. Brádler, in Second European Crystallographic Meeting, Kesthely 1974, Collected Abstracts, p. 124.
[10] M. Polcarová, phys. stat. sol. (a) **46**, 567 (1978); **47**, 179 (1968); **59**, 779 (1980).
[11] M. Polcarová and A. R. Lang, phys. stat. sol. (a) **4**, 491 (1971).
[12] M. Labrune, J. Physique **37**, 1033 (1976).
[13] A. Authier, F. Balibar, Acta Cryst. **A 26**, 647 (1970).
[14] S. Kadečková and B. Šesták, Krist. Tech. **4**, 243 (1969).
[15] M. Polcarová, in Proceedings of V. International Summer School on Defects, Krynica, Poland 1976, edited by Polish Scientific Publishers, Warsaw 1978, p. 393.
[16] M. Renninger, Z. angew. Physik **19**, 20 (1965).